CHAPTER 5

Synthesis of green fluorescent carbon quantum dots via latex of *Ficus benghalensis* for the *detection of tyrosine and fabrication of Schottky barrier diodes*

5.1. Introduction

Tyrosine (4-hydroxyphenylalanine) is an important ingredient of proteins and plays a crucial role in most biochemical reactions [Habibi *et.al*. (2016)]. It is counted as a non-essential amino acid containing a polar group. Tyrosine (Tyr) is a vital precursor for synthesizing melanin, liothyronine, dopamine and catecholamine [Beitollahi *et.al*. (2016)]. During a stressful situation, Tyr is also commonly used to improve learning memory, alertness, attention etc. It creates significant brain chemicals that facilitate nerve cells to communicate and may even regulate mood [Castre *et.al*. (2005)]. It is reported that a typical concentration of Tyr is directly associated with several human diseases. The accumulation of high concentration causes Parkinson's disease or dementia while depression, albinism, alkaptonuria and hypochondria are the common diseases that occurred by a deficiency of Tyr [Shadjou *et.al*. (2018)]. Therefore, a simple, rapid and eco-friendly method is highly demanded to determine Tyr concentration effectively and efficiently. During the last decades, a variety of techniques such as capillary electrophoresis [Wang *et.al*. (2005)], ion-exchange chromatography [Ravindran *et.al*. (2005)], gas chromatography [Nozal *et.al*. (2004)], liquid chromatography [Orhan *et.al*. (2004)], spectrophotoscopy [Azuma *et.al*. (1989)] and electrochemical synthesis [Habibi *et.al*. (2016)], have been applied to determine the concentration of Tyr. Though, these reported techniques require sophisticated instrumentations and mostly time-consuming and costly in nature. Therefore, it is an urgent need to develop a method for the selective and sensitive detection of Tyr. During the past few years, the fluorescence (FL) spectroscopy methods have attracted enormous attention among researchers because of high sensitivity, selectivity and low cost [Zhang *et.al*. (2014)]. The nanoparticles such as AuNPs [Yola *et.al*. (2015)], CeO_2 nanoparticles [Rajavian *et.al*. (2014)], CuO-NPs [Razmi

et.al. (2011)], Graphene quantum dots [Li *et.al*. (2016)], Fe-doped hydroxyapatite nanoparticles [Kanchana *et.al*. (2014)]. etc, have been reported for the detection of Tyr. However, very few reports have been investigated for the sensing of Tyr from carbon quantum dots (CQDs), which are semiconductor nanoparticles with a size of less than 10 nm. CQDs have attracted great attention because of their outstanding properties such as easy surface functionalization, good biocompatibility, low toxicity, good solubility, and tunable excitation-emission properties [Wu *et.al*. (2020), Yang *et.al*. (2020)]. Because of this, CQDs have massive applications in bio-imaging, drug delivery systems, catalysis and sensing of toxic metals [Liu *et.al*. (2020), Bin *et.al*. (2020), Khan *et.al*. (2020), Yang *et.al*. (2020), Gao *et.al*. (2016)]. Based on excellent optical properties of synthesized G-CQDs come under a direct optical band gap region, we have examined the electronic device applicability. To fabricate electronic devices based on synthesized CQDs, has always been a technologically arduous task. Here we have been able to fabricate a Schottky barrier diode on Indium doped tin oxide (ITO) substrate. In electronics, CQDs have so far been applied for various applications such as solar cells [Kirbiyik *et.al*. (2020)], light-emitting diodes [He *et.al*. (2020)]. gas sensor [Liu *et.al*. (2014)]. etc., still to the best of my knowledge, the application of CQDs for the fabrication of a thin-film electronic device, Schottky Barrier Diodes (SBD) have not been reported yet. Various techniques have been applied to synthesize CQDs such as electrochemical synthesis, hydrothermal method, microwave, thermal decomposition, ultrasonic and combustion oxidation. The hydrothermal method is best because of simple operating conditions, low-cost apparatus, low energy consumption and single step [Singh *et.al*. (2018), Rani *et.al*. (2020)]. The doping of heteroatom such as nitrogen in CQDs enhances optical properties like quantum yield, fluorescence (FL) stability, photostability etc, thus broadens the applications in sensing systems. This is probably

because, large conjugated carbon structure broke down and the surface defects of CQDs stabilized because of doping of heteroatom [Kou *et.al.* (2020), Wang *et.al.* (2019), Ju *et.al.* (2014)]. In this manuscript, we have prepared tunable fluorescent green carbon quantum dots (G-CQDs) from the latex of Ficus benghalensis as a carbon source and polyethyleneimine as a nitrogen source through one-pot hydrothermal synthesis (**Scheme 5.1**).

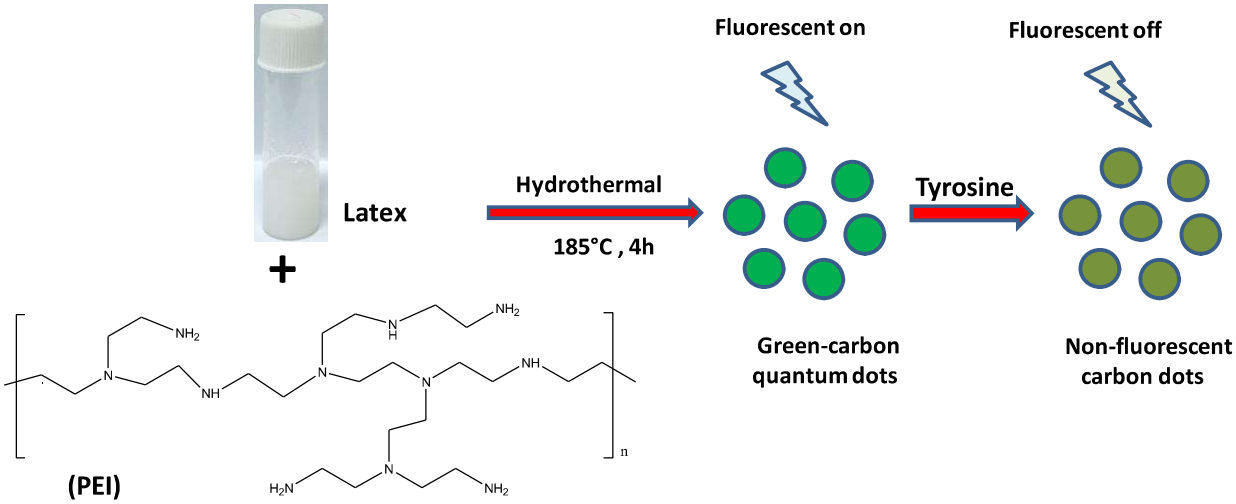

Scheme 5.1 The Synthetic methodology was adopted for one-pot hydrothermal treatment of G-CQDs.

The as-prepared G-CQDs have been entirely characterized via various instrumental techniques like TEM, P-XRD, FT-IR, Zeta potential, XPS, UV-Vis and fluorescence spectroscopy. Besides, the fluorescence stability of G-CQDs has been analyzed in a variety of

parameters like pH, a higher concentration of NaCl and keeping G-CQDs at room temperature for approximately eight months. These prepared G-CQDs have been utilized for the selective and sensitive detection of Tyrosine (Tyr) with a good quantum yield. Further, the detection of Tyr has been performed in the milk sample with superior recovery. We have also fabricated a thin-film electronic device, a Schottky barrier diode by using G-CQDs. The findings open a fresh channel for the CQDs applicability in the field of electronics.

5.2. Experimental section

5.2.1. Chemical and materials

The latexes of Ficus benghalensis were obtained from the campus of Banaras Hindu University, Varanasi, India. Polyethyleneimine and metals used for sensing purposes were purchased from Sigma Aldrich, India. The amino acids such as leucine (Leu), asparagine (Asn), tryptophan (Trp), cysteine (Cys), tyrosine (Tyr), threonine (Thr), proline (Pro), serine (Ser), isoleucine (IIe), valine (Val) and phenylalanine (Phe) were procured from Avra chemical limited.

5.2.2. Synthesis of Green Carbon Quantum dots (G-CQDs)

In general, 500 µL latex was mixed with 150 mL of de-ionized water in a flask and 1mL polyethyleneimine was added in this suspension and sonicated for 20 minutes. Poured the obtained reaction mixture into a 250 mL Teflon lined stainless steel autoclave chamber and heated in a hydrothermal oven for 4 hours at 185°C. As the process finished, the autoclave was settled for cooling at room temperature. The obtained brown colour solution was filtered and centrifuged filtrate at 18000 rpm for 15 minutes. Finally dialyzed the supernatant solution through a previously reported method [Yadav *et.al*. (2019)].

5.2.3. Determination of quantum yield (QY)

Quinine sulfate (Quantum Yield = 54% in H_2SO_4 solution, concentration = 0.1 M, at 360 nm) was taken as a standard sample and QY was calculated from **equation 5.1** of **Table 5.1.**

5.2.4. Apparatus and Characterization

The ultra-violet visible (UV-vis) absorption spectra were conducted on (EVOLUTION 201, Thermo Scientific) spectrophotometer at 200-800 nm. The FL spectra were performed on Edinburgh instrument FLS 980 fluorescence spectrophotometer. TEM was carried out on a (TEM, TECHNAI 20 G2) at the accelerating voltage of 200 kV. The Zeta potential of G-CQDs has been carried out on the Nano Zeta Sizer Malvern apparatus (4.0 mW laser). XRD was conducted on a Rigaku Smart lab between 2θ = 5-80°. The Fourier Transform Infra-red (FT-IR) Spectrum was recorded on KBr pellets with Perkin Elmer Spectrum 100. The (AMICUS, Kratos Analytical, A Shimadzu) instrument was used for the X-ray photoelectron spectroscopy (XPS).

5.2.5. Device fabrication

For metal-semiconductor (MS) junction device fabrication, Indium doped Tin oxide (ITO) coated glass substrates (15×15 mm^2) are ultrasonically cleaned using a wet cleaning process. The cleaned ITO substrates are dried for 30 minutes in a micro-oven at 100°C, and finally processed by plasma cleaning in presence of argon and oxygen for 20 min. Initially, Green Carbon quantum dot (G-CQDs) dispersed in de-ionized water was deposited on the ITO coated glass substrate and annealed at 100^0C for two hours and this process is repeated to obtained desired thickness of G-CQDs (~100 nm). In the second step, ~80 nm thick metal (Ag) was deposited for a contact electrode by using a thermal evaporator unit. The evaporated metal (Ag) forms the

circular dots of a 1 mm radius on the top of the G-CQDs coated ITO substrate using a shadow mask technique [Upadhyay *et.al*. (2018)]. The thickness (~100 nm) was examined by the F20 Filmmetrics, USA instrument.

5.3. Result and discussion

The TEM of as-prepared G-CQDs showed the spherical morphology (**Figure 5.1a**) and the corresponding histogram reveals that the size of G-CQDs distributed from 1 to 6 nm with an average size of 3.7 nm (**Figure 5.1b**). The inset **Figure 5.1a** is the SAED pattern that reveals the amorphous nature of G-CQDs which was further proved by the XRD pattern with broadband at 2θ = 24.7° **(Figure 5.1c)** [Rani *et.al*. (2020)]**.** The FT-IR spectrum demonstrates the surface functionality of G-CQDs (**Figure 5.1d**). The peaks at 3433 cm^{-1} affirm the presence of O-H/N-H groups. The band at 2982 cm^{-1} corresponded to –CH stretching vibrations, While the peaks at 1710, 1446 and 1632 cm^{-1} attributed to C=O, C=C stretching and N-H bending, respectively. The bands near 1373 and 1202 cm^{-1} were because of C-N and C-O, respectively. All these results revealed various functional moieties on G-CQDs surface. [Han *et.al*. (2015), Wang *et.al*. (2019) Yue *et.al*. (2020), Zhao *et.al*. (2029), Gao *et.al*. (2015)].

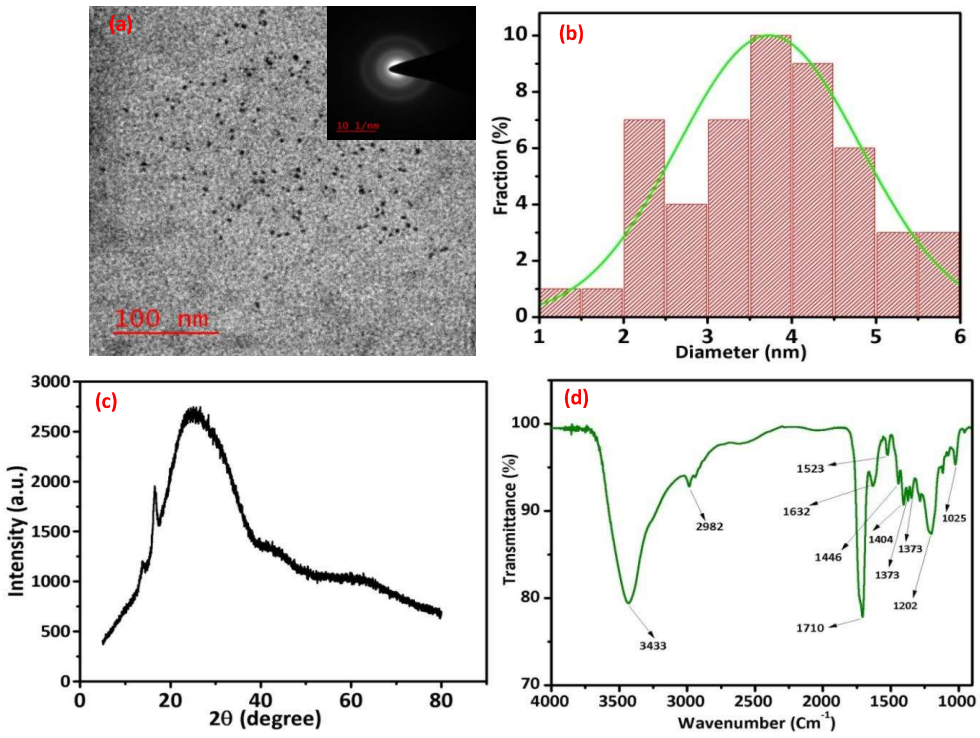

Figure 5.1 (a) TEM figure of synthesized G-CQDs, (b) Size distribution histogram, (c) XRD spectra of the G-CQDs and (d) FT-IR spectra of G-CQDs.

The XPS spectrum further confirms the above functional groups in G-CQDs. **Figure 5.2a** is the bride survey XPS spectrum showing the presence of C1s (285.67 eV), N1s (397.96 eV) and O1s (530.61 eV) in G-CQDs. The standard uncharged binding energy of C1s is 284.8 eV. Therefore, correction in C peak has been performed by 0.94eV **(Figure 5.2b).** The contents of carbon, oxygen and nitrogen in the sample were found to be 56.39% (C), 36.15% (O) and 7.45 % (N) respectively, revealing a good doping concentration of N in G-CQDS. The corrected C1s has three peaks corresponding to C-C/C=C at 282.84 eV, C-N/C-O at 284.73 eV, and C=O/C=N at 285.12 eV (**Figure 5.2b**) [Ju *et.al*. (2015)]. The presence of C-N-C groups (397.60 eV), pyrrolic N (398.82 eV) and pyridinic N (398.18 eV) was confirmed by N1s spectrum (**Figure 5.2c**). [Bin

et.al. (2020)]. The O1s spectrum splits into three components which apparent the existence of C=O (530.67 eV), N=O (531.92 eV) and (C-OH/C-O-C) at 531.22 eV (**Figure 5.2d**) [Yang *et.al*. (2020)].

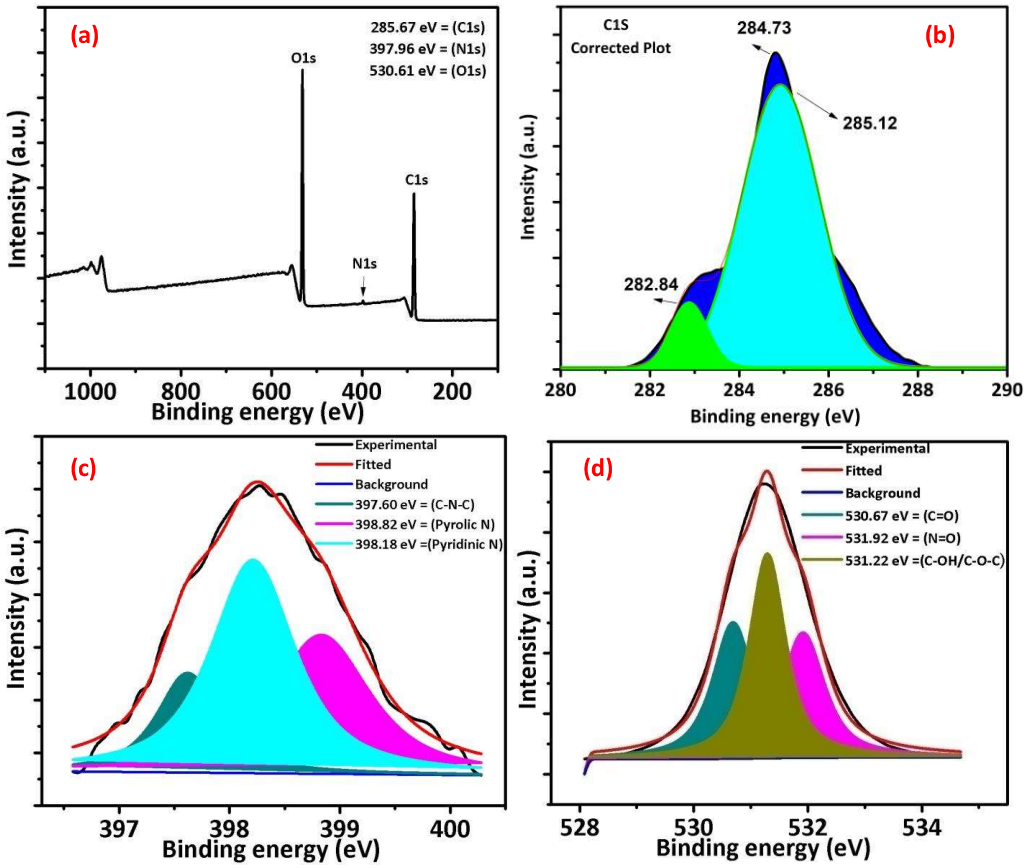

Figure 5.2 XPS survey spectrum (a), Corrected C1s spectra (b), N1s (c), and O1s (d), of the as-prepared G-CQDs.

The charge on G-CQDs was -16 mV which was determined by zeta potential (**Figure5.3).**

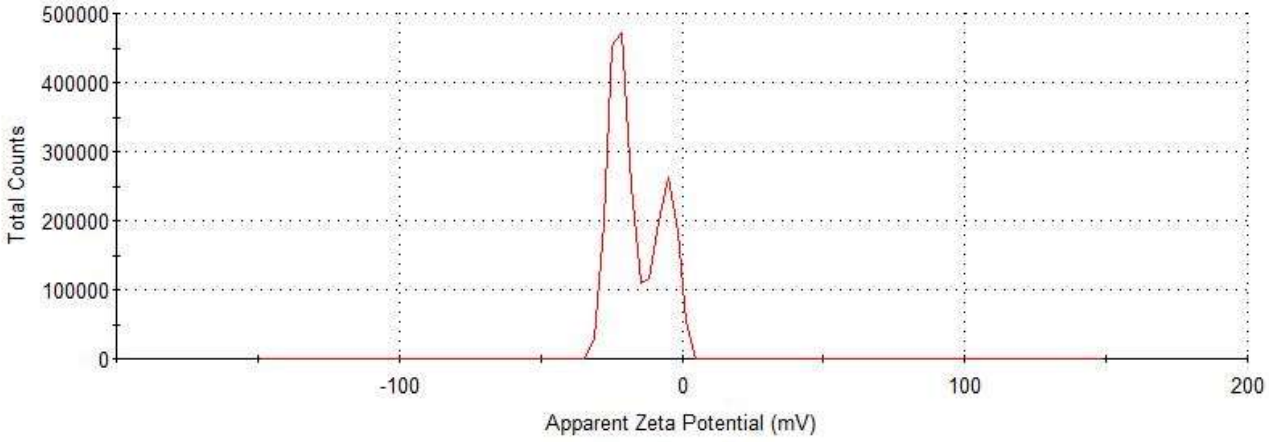

Figure 5.3 Zeta potential of as-synthesized G-CQDs.

5.4. Optical properties

The G-CQDs exhibited two absorption bands at 298 nm and 349 nm due to π-π* transition of conjugated skeletons and n−π* of a heteroatom-containing bond respectively [Wu *et.al*. (2020)] **(Figure 5.4a).** The as-synthesized G-CQDs display excitation dependent emission. This is probably because of excitons of carbon, surface states, free zig-zag sites and emissive traps [Zhang *et.al*. (2014)]. As the excitation wavelength increases from 310 to 390 nm, the emission intensity increases. The maximum emission intensity obtained was 527 nm at the excitation of 390 nm. After then, a gradual decrease in the emission intensity was observed as the excitation increases from 390 to 440 nm **(Figure 5.4b).** The as-synthesized G-CQDs exhibited green colour under UV- light at the excitation of 365 nm. The International Commission on

Illumination (CIE) diagram further confirms the green colour with CIE coordinate located at (0.28, 0.48) **(Figure 5.4c).**

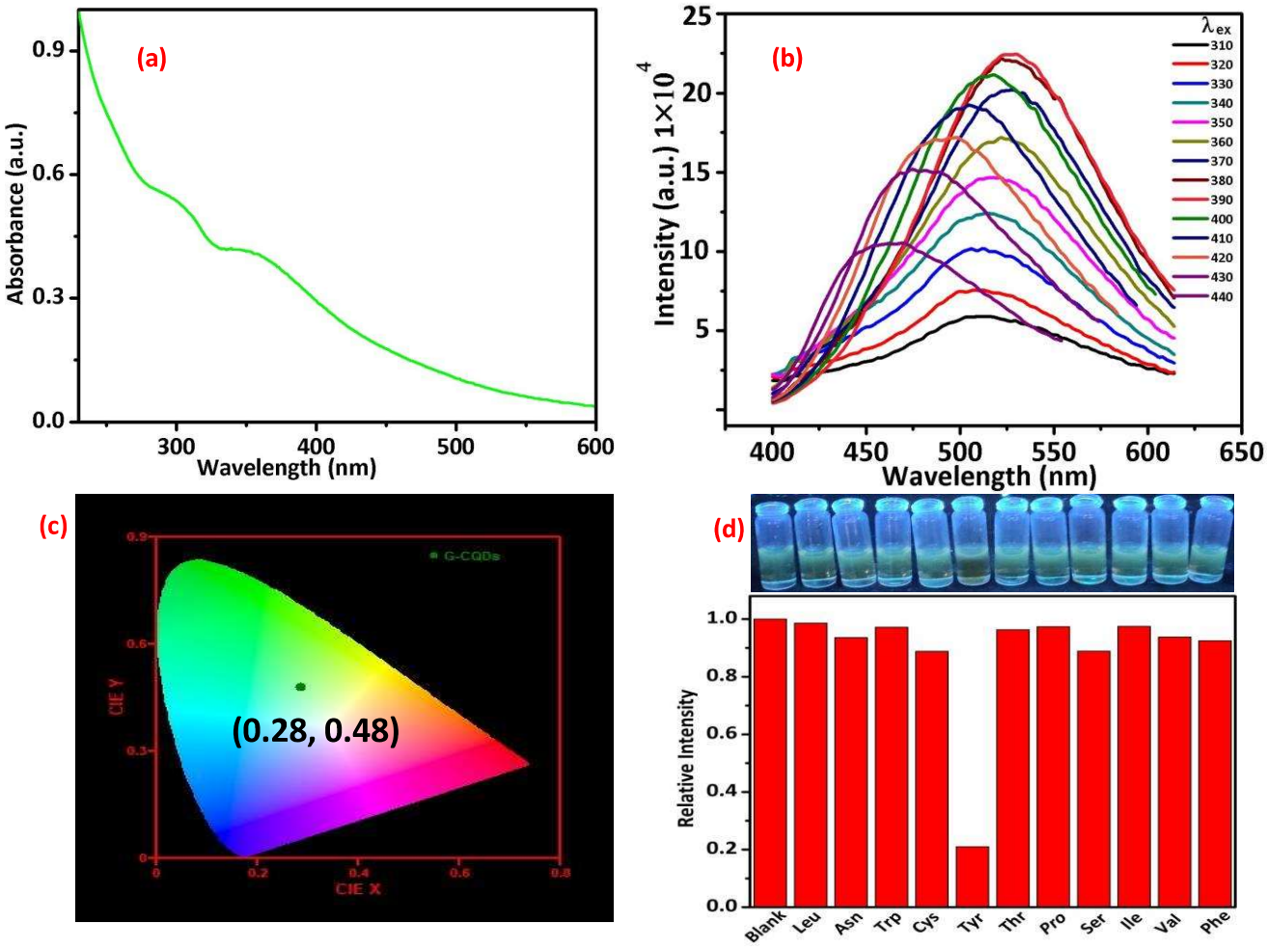

Figure 5.4 (a) UV-visible absorption spectrum of G-CQDs. (b) FL emission of G-CQDs at different excitation wavelength (310-440 nm). (c) Image of CIE coordinates showing the green colour of G-CQDs. (d) Photograph illustrating selective sensing of Tyr and bar diagram represents relative fluorescence intensity of G-CQDs after addition 50 µL of Tyr (1 x 10^{-3}M) and other amino acids (1x 10^{-2} M) designated negligible interference of other amino acids.

The quinine sulphate (QY, 54%) was taken as a standard to calculate the quantum yield (QY) and was calculated to be 41.2% **(Table 5.1).**

Table 5.1. Calculation of fluorescence quantum yield with integrated intensity and absorbance of quinine sulfate and G-CQDs at excitation wavelength 360 nm.

Sample	Integrated intensity at 360 nm	Absorbance at 360 nm	Quantum yield (%)
Quinine sulphate (reference)	51246927	0.076	54
G-CQDs	38087271	0.074	41.2

Following **equation 5.1** was used to calculate quantum yield-

$$QY = QY_{Ref} \cdot \frac{I}{A} \cdot \frac{A_{Ref}}{I_{Ref}} \cdot \frac{\eta^2}{\eta^2_{Ref}} \qquad \textbf{5.1}$$

Where QY and QY_{ref} are quantum yield of G-CQDs and reference respectively, I is the integrated intensity, A is the absorbance and η is the refractive index ($\eta^2/\eta^2_{ref}=1$) of the solvent.

Further, investigated the effect of pH and ionic strength on the fluorescence intensity of G-CQDs. It can be seen from **Figure 5.5** that as the pH increases from 2 to 9, emission intensity

increases and after achieving maximum intensity at pH 9, a slight decrease in the intensity was observed, revealing that G-CQDs are stable in a wide pH range. To observe the effect of ionic strength on G-CQDs fluorescence intensity, various strengths of KCl solutions (0.5 to 5 M) were made and treated with G-CQDs solution. No obvious shift in the fluorescent intensity was observed, enlightening strong stability of groups present in G-CQDs surface (**Figure 5.6**). No precipitations were obtained when G-CQDs kept at room temperature for around eight months, instructive long-term stability.

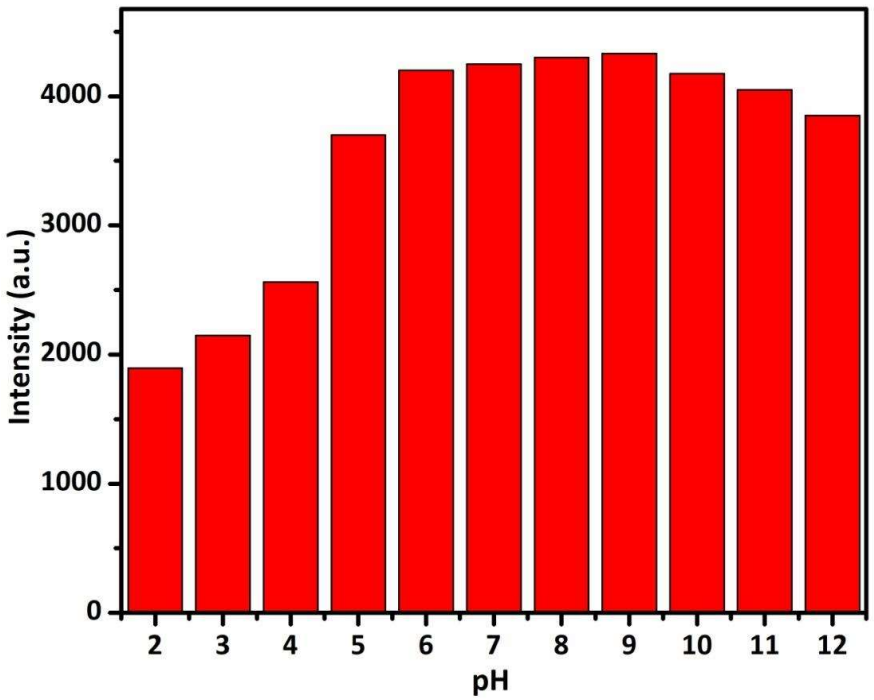

Figure 5.5 Study of pH change on the fluorescent intensity of G-CQDs with corresponding photograph under UV – light (λex = 365 nm) from pH range 2 to 12.

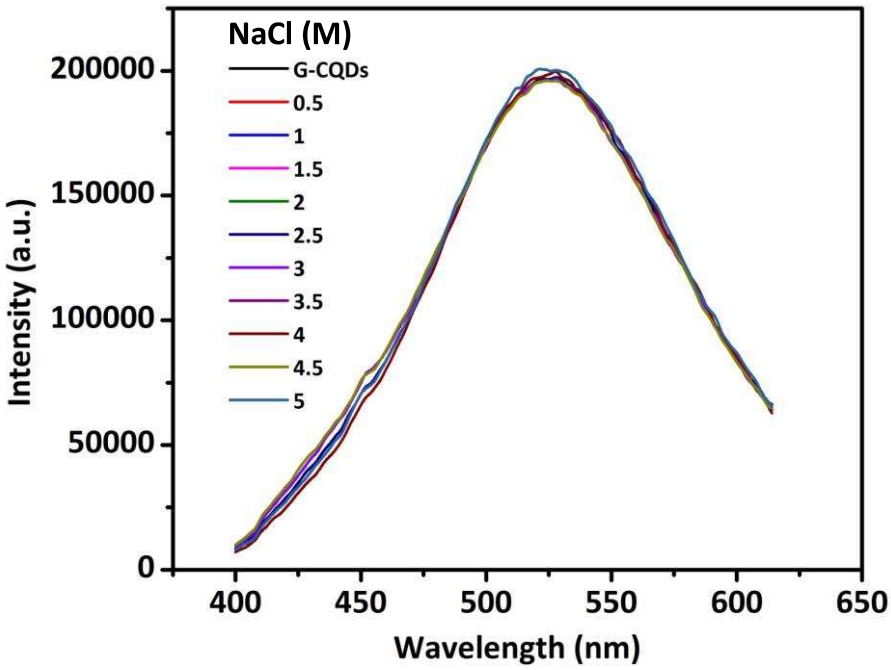

Figure 5.6 Effect of ionic strength on the fluorescent intensity of G-CQDs.

5.5. Selectivity studies

Selectivity is an essential parameter to assess the sensing activities. Consequently, interference of different amino acid (Leu, Asn, Trp, Cys, Tyr, Thr, Pro, Ser, IIe, Val and Phe) has been investigated by fluorescence spectrophotometer and results signify that out of these amino acids, G-CQDs selectively detect Tyr (**Figure 5.4d).** Further, the influence of different metal ions (Cu^{+}, Ag^{+}, Na^{+}, K^{+}, Al^{3+}, Ni^{2+}, Fe^{2+} Pb^{2+}, Cd^{2+}, Cr^{3+}, Hg^{2+}, Co^{2+} and As^{3+}), on the fluorescence intensity of G-CQDs was observed. First of all, in 3 mL of G-CQDs solution (C, 30

mg mL^{-1}), 50 µL of different metal ions (C, $1x10^{-2}$ M) were added and was found almost no obvious effect on the fluorescence intensity of G-CQDs **(Figure 5.7).**

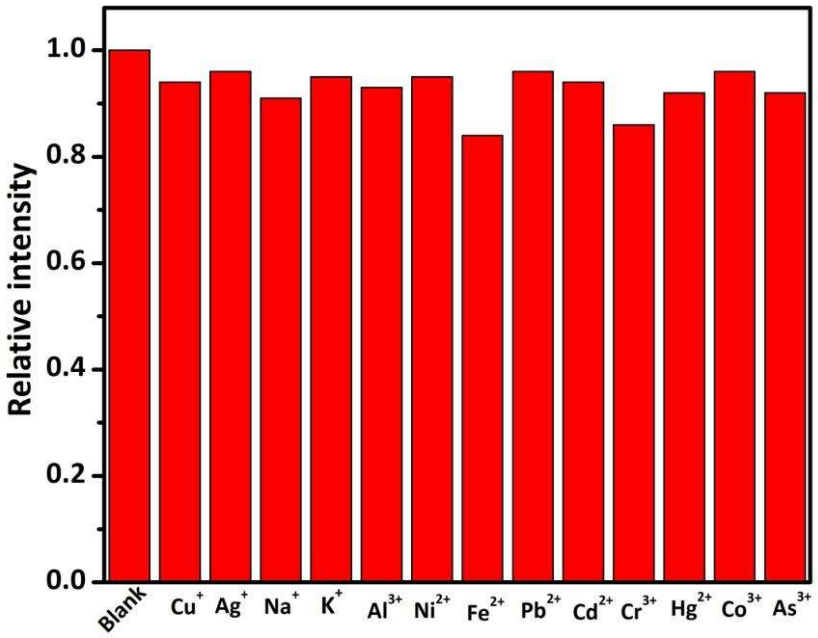

Figure 5.7 Influence of metal ions on the fluorescence of G-CQDs.

The sensitivity experiment of G-CQDs fluorescent probe towards Tyr detection was performed by a fluorescent titration experiment with exciting G-CQDs at its maximum excitation wavelength (390 nm). Upon gradual addition of 50 µL Tyr (C, top to bottom: 0, 15, 30, 45, 60, 75, 90, 100 µM), into G-CQDs solution (30 mg mL^{-1}), the maximum fluorescent intensity (525nm) continuously decreases. (**Figure 5.8a).**

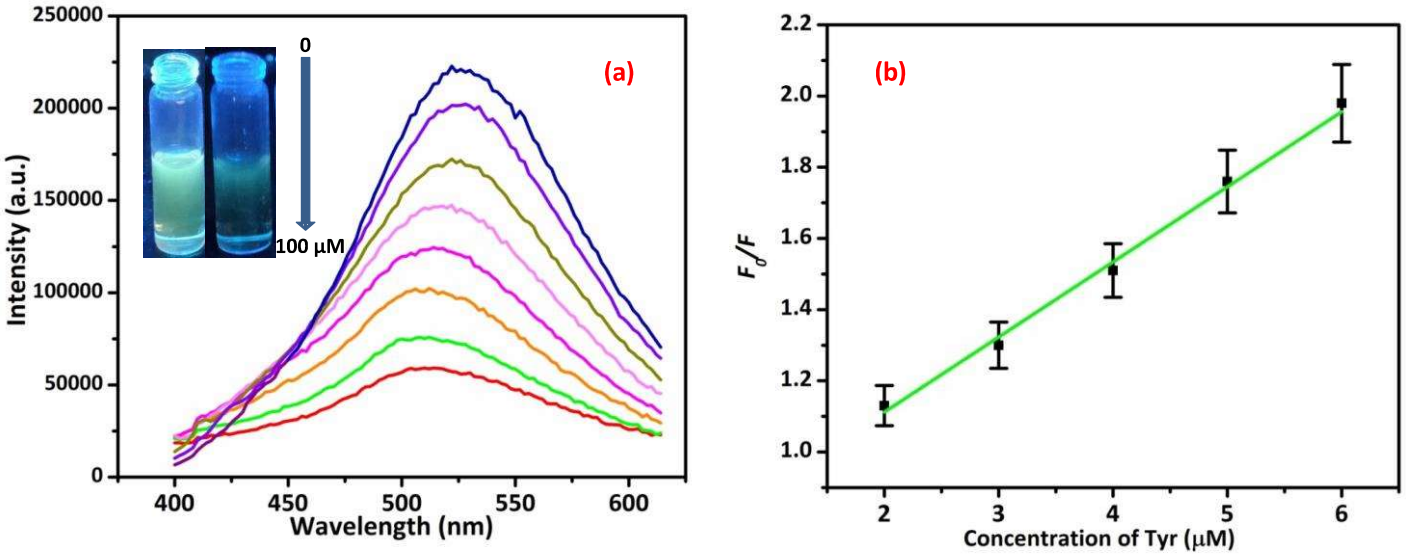

Figure 5.8 (a) FL titration experiment enlightening the quenching upon successive addition of 50 µL Tyr (C, top to bottom: 0, 15, 30, 45, 60, 75, 90, 100 µM) into G-CQDs solution (30 mg mL^{-1}). (b) Fluorescent detection of Tyr being fitted into Stern-Volmer plot.

To understand mechanism effectively, the G-CQDs were excited at their highest exciting wavelength (390 nm) during FL titration experiments. On adding Tyr solutions (0 to 100 µM) gradually, maximum emission intensity at 525 nm continuously decreases, revealing the interaction of G-CQDs with Tyr. The selectivity might be due to the specific affinity amid amino/carboxyl groups on G-CQDs surface and Tyr. In addition, Tyr could be oxidized to dopaquinone through tyrosinase catalyzation, which could efficiently quench the PL of G-CQDs through electron transfer process [Li *et.al*. (2016)]. Besides this, the quenching maybe because of the inner filter effect, dynamic quenching or static quenching. It is clear from **Figure 5.9a** that the UV-Visible absorption spectra of Tyr have a peak at 273 nm (black line). The as-prepared G-

CQDs exhibited an excitation band centred at 390 nm (blue line) and a maximum emission band at 525 nm (green line). Therefore, no spectral overlap has been observed between absorber (Tyr) and fluorophore of G-CQDs, revealing the non-occurrence of the inner filter effect.

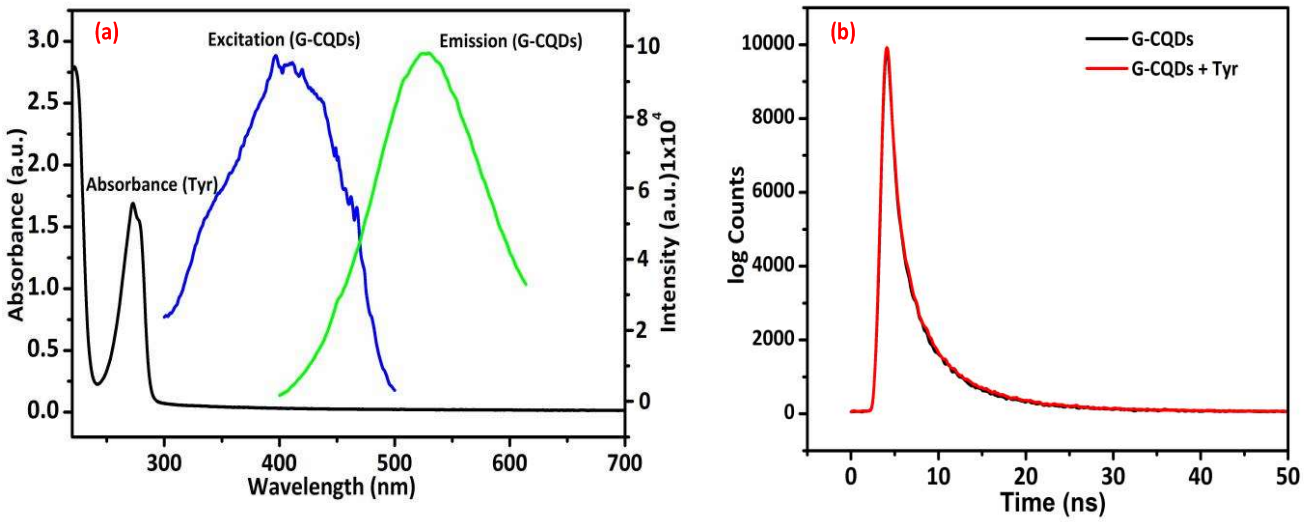

Figure 5.9 (a) Absorption spectra of Tyr (black line), excitation (blue line) and emission (green line) spectra of G-CQDs. (b) FL lifetime decay curves of G-CQDs in the absence and presence of Tyr.

To confirm the FL quenching of G-CQDs, the lifetime measurements experiment has been performed in the presence/absence of Tyr. From **Figure 5.9b** and **Table 5.2**, it is clear that the fluorescence decay outlines were fitted by a triexponential aspect having average lifetime value 5.34 ns and 5.18 ns for G-CQDs and G-CQDs Tyr respectively. There was almost no noticeable alteration in the life-time after adding Tyr, revealing the ground state interaction

between fluorophore (G-CQDs) and quencher (Tyr). This result illustrates the static quenching [LeCroy *et.al*. (2017)].

Table 5.2 Fluorescence lifetime measurement of G-CQDs in the presence and absence of Tyrosine.

Compound	Average life time (ns)	Chi square	Different life time (ns)	Corresponding Weight (%)
G-CQDs	5.34	1.07	τ_1 = 1.03 (B_1=5421.42) τ_2 = 4.06 (B_2=4657.10) τ_3 = 10.5 (B_3=787.87)	17.06 57.68 25.26
G-CQDs + Tyr	5.18	1.20	τ_1 = 1.02 (B_1=5323.23) τ_2 = 3.89 (B_2=4541.37) τ_3 = 9.77 (B_3=1125.83)	15.91 51.86 32.23

The fluorescence life time decay of G-CQDs was fitted by a tri-exponential role. Chi-square standards and corresponding residual division were reduced to judge the best fit. The adequate fit has a chi-square close to unity.

The fitting system of the fluorescence emission intensity decay $I_{(t)}$ uses a tri-exponential representation according to the following **equation 5.2.**

$$I_{(t)} = B_1 \exp(- t / \tau_1) + B_2 \exp(-t / \tau_2) + B_3 \exp(-t / \tau_3) \quad \textbf{5.2}$$

Where τ_1 , τ_2 and τ_3 represents time constants of the three radiative decays channel and B_1, B_2 , B_3 are three corresponding amplitudes.

To calculate the average life time, following **equation 5.3** was used -

$$< \tau > = \frac{B_1 \tau_1^2 + B_2 \tau_2^2 + B_3 \tau_3^2}{B_1 \tau_1 + B_2 \tau_2 + B_3 \tau_3} \quad \textbf{5.3}$$

This quenching was additionally supported with a photograph taken under UV-light (λex = 365nm) **(Inset Figure 5.8a).** The FL quenching effectiveness was well fitted by Stern-Volmer **equation 5.4**.

$$F_0 / F = 1 + k_{sv}.[Q] \quad \textbf{5.4}$$

Where F_0 represents the FL intensity of G-CQDs, F is the FL intensity of G-CQDs in the presence of quencher (Tyr), Q is the concentration of quencher, and k_{sv} symbolize quenching constant. The k_{sv} value of as-synthesized G-CQDs was estimated to be 0.21107 $(\mu M)^{-1}$ with a correlation coefficient (R^2) of 0.9925. Furthermore, F_0 / F linearly depends on the Tyr concentration in the range of 2 to 6 μM **(Figure 5.8b).** The LOD was calculated to be 0.13 μM with a signal to noise ratio of 3 which was comparable to an earlier reported method. (**Table5.3**) [Yang *et.al*. (2014), Chai *et.al*. (2015), Ao *et.al*. (2016), Teng *et.al*. (2015), Hu *et.al*. (2017)].

Table 5.3 Comparison of Sensing performance with other nanoprobes.

Detection probe (C-based)	Detection limit (µM)	Linear range (µM)	Quantum yield (%)	Reference
AuNCs@Tyr	80.0	500-20000	2.5	42
Dopa-CQDs	7.0	23.2 -793.5	1	43
Dopa-Au/Ag NCs	13.5	45-319.5	-	44
AuNCs	6.0	6-3600	-	45
CQDs-Dopa	17.7	44.4-711	2.1	46
G-CQDs	0.13	2- 6	41.2	**Present work**

Addition to this, the sensing of tyrosine was further performed in milk sample. The milk sample spiked with various concentrations of Tyrosine. Result shown in **Table 5.4** revealed that the detection efficiency of Tyr varied from 91.2 to 93.4**%** with good recovery efficiency (RSD = 92.72 ± 1.69%).

Table 5.4 Detection of Tyr in milk sample by using G-CQDs.

Added (µM)	Found (µM)	Recovery (%)
25	22.8	91.2 %
50	47.3	94.6 %
75	68.8	91.7%
100	93.4	93.4%

RSD = 92.72 ± 1.69%

5.6. The strategy of device fabrication

By using the above optical property of synthesized green carbon quantum dots (G-CQDs), a Schottky diode was designed as shown in **Scheme 5.2**.

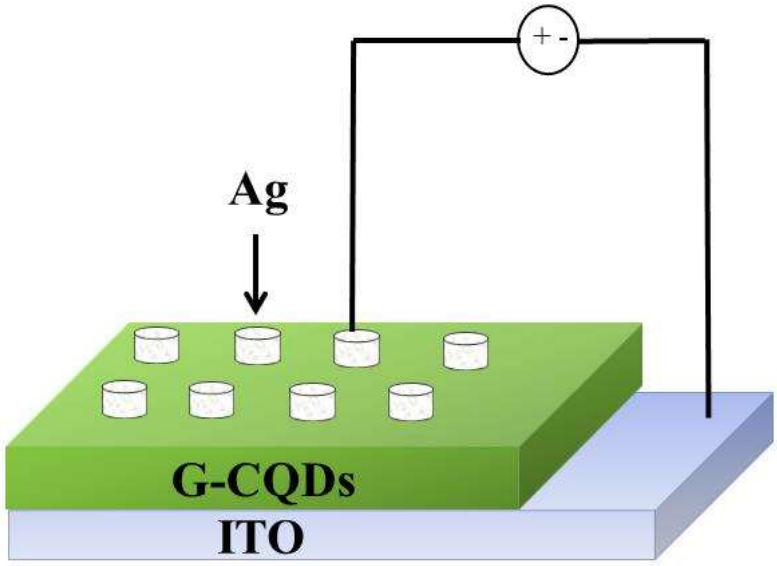

Scheme 5.2 Schematic presentation of fabrication of Schottky barrier diode based on G-CQDs.

We have fabricated a metal (Ag)–Semiconductor Carbon Quantum Dots G-CQDs junction based thin-film device and investigated the current-voltage (*I-V*) characteristics of the device. The (*I–V*) measurements of G-CQDs based thin-film device were examined with the help of the semiconductor parameter analyser from -1.5 V to +1.5 V at room temperature. *I–V* characteristics of fabricated devices have been examined, as shown in **Figure 5.10.**.

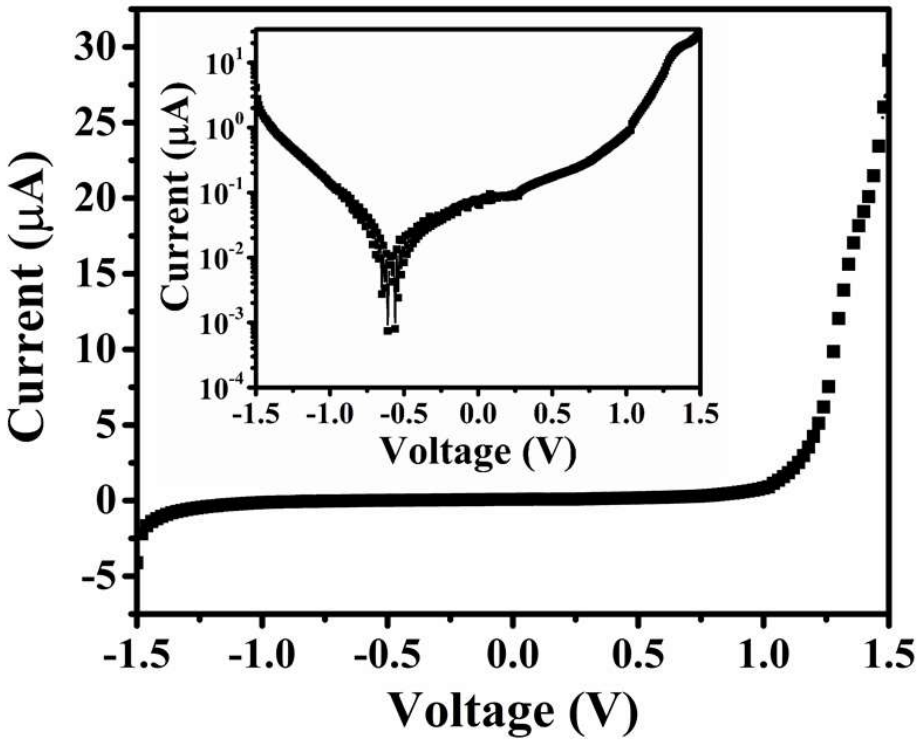

Figure 5.10. *I–V* characteristics graph for ITO/G-CQDs/Ag-based Schottky Barrier diode.

By using *I–V* characteristics of the Ag/G-CQDs based thin-film device, the interface between Ag/G-CQDs exhibits a nonlinear rectifying behaviour, which indicates the formation of a Schottky Barrier diode. The obtained current-voltage (*I-V*) characteristics of G-CQDs were further analyzed by assuming the standard thermionic theory and Cheung's equation [Dhibar *et.al*. (2018), Kumar *et.al*. (2021)], and calculated key parameters of the fabricated device. To analyze the I-V graph, we have first employed the following standard equations:

$$I = I_0 \exp\left(\frac{qV}{\acute{\eta}KT}\right)\left(1 - \exp\left(-\frac{-qV}{\acute{\eta}KT}\right)\right) \qquad \textbf{5.6}$$

At room temperature, reverse saturation current density J_0<<1, Therefore

$$I_0 = AA^* T^2 \exp(\frac{-q\phi_B}{KT}) \quad 5.7$$

$$\phi_B = \frac{KT}{q} ln(\frac{A^* T^2}{J_0}) \quad 5.8$$

Where I_0, A, and A* stand for reverse saturation current, schottky diode area, and Richardson constant, respectively. The Schottky diode area was calculated as 3.14×10^{-6} m^2 and Richardson constant was considered as 32 A K^{-2} cm^{-2} for the G-CQDs based devices. The estimated value of reverse saturation current was 4.2 x 10^{-9} A and the value of the measured barrier height (ϕ_B), for the synthesized G-CQDs based SBD is ~0.79 eV.

5.7. Conclusion

In summary, we have synthesized fluorescent G-CQDs through one-pot hydrothermal method using the latex of ficus benghalensis and polyethyleneimine. The as-synthesize G-CQDs exhibited excitation-dependent emission with a high QY of 41.2%. G-CQDs are stable in a wide pH range and showed high photostability and are also stable in high salt conditions. The G-CQDs were employed to detect Tyr with good selectivity and sensitivity with a detection limit of 0.13 μM. Further, the detection of Tyr was performed in the milk sample. In addition, the ITO/G-CQDs/Ag-based Schottky Barrier Diode is fabricated and characterized for current-voltage (*I–V)* characteristics at room temperature, and obtained value of reverse saturation current (I_0), and barrier height (ϕ_B), for fabricated Schottky barrier diode was~ 4.2 x 10^{-9}A, ~ 0.79 eV respectively. Thus, the present study of ITO/G-CQDs/Ag advocates the future possibility of achieving G-CQDs based electronic devices for advanced technology.